Acta Biomaterialia 86 (2019) 280–290

Contents lists available at ScienceDirect

Acta Biomaterialia

journal homepage: www.elsevier.com/locate/actabiomat

Full length article

In situ chemically crosslinked injectable hydrogels for the subcutaneous delivery of trastuzumab to treat breast cancer

Yu-Wen Lo [a,b,1], Ming-Thau Sheu [a,1], Wen-Hsuan Chiang [b], Ya-Ling Chiu [b], Chia-Mu Tu [b], Wen-Yu Wang [b], Ming-Hsi Wu [b], Yu-Cheng Wang [b], Maggie Lu [b,*], Hsiu-O Ho [a,*]

[a] School of Pharmacy, College of Pharmacy, Taipei Medical University, Taipei, Taiwan
[b] Biomedical Technology and Device Research Laboratories, Industrial Technology Research Institute, Hsinchu, Taiwan

ARTICLE INFO

Article history:
Received 23 August 2018
Received in revised form 18 December 2018
Accepted 4 January 2019
Available online 05 January 2019

Keywords:
Injectable hydrogels
Sustained release
Maleimide-modified γ-polyglutamic acid
Thiol end-functionalized 4-arm poly (ethylene glycol)
Trastuzumab

ABSTRACT

Recently, novel approaches for the delivery of therapeutic antibodies have attracted much attention, especially sustained release formulations. However, sustained release formulations capable of carrying a high antibody load remain a challenge for practical use. In this study, a novel injectable hydrogel composed of maleimide-modified γ-polyglutamic acid (γ-PGA-MA) and thiol end-functionalized 4-arm poly (ethylene glycol) (4-arm PEG-SH) was developed for the subcutaneous delivery of trastuzumab. γ-PGA-MA and 4-arm PEG-SH formed a hydrogel through thiol-maleimide reactions, which had shear-thinning properties and reversible rheological behaviors. Moreover, a high content of trastuzumab (>100 mg/mL) could be loaded into this hydrogel, and trastuzumab demonstrated a sustained release over several weeks through electrostatic attraction. In addition, trastuzumab released from the hydrogel had adequate stability in terms of its structural integrity, binding bioactivity, and antiproliferative effect on BT-474 cells. Pharmacokinetic studies demonstrated that trastuzumab-loaded hydrogel (Her-hydrogel-10, composed of 1.5% γ-PGA-MA, 1.5% 4-arm PEG-SH, and 10 mg/mL trastuzumab) and trastuzumab/Zn-loaded hydrogel (Her/Zn-hydrogel-10, composed of 1.5% γ-PGA-MA, 1.5% 4-arm PEG-SH, 5 mM $ZnCl_2$, and 10 mg/mL trastuzumab) could lower the maximum plasma concentration (C_{max}) than the trastuzumab solution. Furthermore, Her/Zn-hydrogel-10 was better able to release trastuzumab in a controlled manner, which was ascribed to electrostatic attraction and formation of trastuzumab/Zn nanocomplexes. In a BT-474 xenograft tumor model, Her-hydrogel-10 had a similar tumor growth-inhibitory effect as that of the trastuzumab solution. By contrast, Her/Zn-hydrogel-10 exhibited a superior tumor growth-inhibitory capability due to the functionality of Zn. This study demonstrated that this hydrogel has potential as a carrier for the local and systemic delivery of proteins and antibodies.

Statement of Significance

Recently, novel sustained-release formulations of therapeutic antibodies have attracted much attention. However, these formulations should be able to carry a high antibody load owing to the required high dose, and these formulations remain a challenge for practical use. In this study, a novel injectable chemically cross-linked hydrogel was developed for the subcutaneous delivery of trastuzumab. This novel hydrogel possessed ideal characteristics of loading high content of trastuzumab (>100 mg/mL), sustained release of trastuzumab over several weeks, and maintaining adequate stability of trastuzumab. In vivo studies demonstrated that a trastuzumab-loaded hydrogel possessed the ability of controlled release of trastuzumab and maintained antitumor efficacy same as that of trastuzumab. These results implied that a γ-PGA-MA and 4-arm PEG-SH-based hydrogel has great potential in serving as a carrier for the local or systemic delivery of therapeutic proteins or antibodies.

1. Introduction

Therapeutic monoclonal antibodies (Abs; mAbs) have occupied a major role in pharmaceutical development pipelines, especially

* Corresponding authors.
E-mail addresses: MaggieLu@itri.org.tw (M. Lu), hsiuoho@tmu.edu.tw (Hsiu-O Ho).
[1] These authors contributed equally to this work.

https://doi.org/10.1016/j.actbio.2019.01.003
1742-7061/

in the areas of cancer and inflammation. More than 50 mAbs were under late-stage clinical trials in 2016, and over 70 mAbs will be on the market with estimated global sales of US$125 billion by the end of 2020 [1,2]. To date, the majority of mAbs are injected through the intravenous (IV) route, thus requiring huge doses, which lead to patient inconvenience and high medical treatment costs. Therefore, regional injection of mAbs for systemic or local treatment might be an efficient strategy for delivering mAbs.

Several novel strategies for delivering mAbs were recently developed. Hyaluronidase (rHuPH20) can temporarily degrade hyaluronan in the subcutaneous (SC) region, thus leading to a five-fold increase in the allowable injection volume and improving the bioavailability of mAbs [3]. Herceptin® (trastuzumab) or MABTHERA® (rituximab) combined with rHuPH20 was successfully developed as an SC product on the market in 2013 and 2014, respectively. In addition, an intra-articular injection of anti-tumor necrosis factor (TNF)-α Ab exhibited prolonged drug exposure and improved efficacy in arthritis treatment [4–6]. Furthermore, controlled release systems of Abs through microparticles or injectable hydrogels are capable of increasing drug exposure times in desired regions, thus enhancing therapeutic efficacies and reducing high drug concentration-related side effects. For instance, an intravitreal (IVT) injection of vascular endothelial growth factor (VEGF) Ab-loaded sustained release formulations could maintain effective drug concentrations for several months and possess therapeutic advantages in treating age-related macular degeneration (AMD) [7–9]. Local sustained release of an epidermal growth factor receptor (EGFR) Ab (trastuzumab) or VEGF Ab (bevacizumab) through an injectable hydrogel enhanced the anti-tumor efficacy [10–12]. Moreover, cancer immunotherapy using checkpoint-blocking antibodies such as a programmed death (PD)-1 Ab and cytotoxic T-lymphocyte-associated protein (CTLA)-4 Ab exhibited promising antitumor efficacies compared to existing cancer treatments. However, these Abs resulted in many side effects termed immune-related adverse events (irAEs) [13]. Local slow release formulations indicated that low doses of immunomodulatory Abs were capable of inducing sufficient immune responses, as well as systemic high doses, without leading to adverse effects [14–16].

Despite previous great achievements in providing better Ab delivery strategies, challenges still exist in the clinical use of these formulations. High Ab loading of sustained release formulations is an important requirement for clinical use due to a limited injection volume for SC (ca. 1.5 mL) and IVT (ca. 0.05 mL) injections [17,18]. Hydrogel formulations are extremely versatile drug delivery vehicles for small molecules and biological macromolecules and possess wide applications. For examples, active molecule-encapsulated pH-responsive/self-healing hydrogels are suitable for oral delivery, cancer treatment, and wound dressing [19–21]. Injectable gel formulations also have an advantage compared to microparticle formulations because they provide high protein loading of >30% [22]. Moreover, mAbs in hydrogels still maintain their structural integrity and bioactivity for several weeks [8–12,23,24]. More importantly, injectable hydrogel-encapsulated therapeutic Abs based on electrostatic interactions exhibit Ab sustained release with characteristics of lowering the maximum plasma concentration (C_{max}) and postponing the time to the maximum concentration (T_{max}) [12,23,24]. γ-Polyglutamic acid (γ-PGA), composed of repeating units of glutamic acid connected by amide linkages between α-amino and γ-carboxyl groups, is an anionic and biodegradable biopolymer that has been applied in drug delivery, biological adhesives, food industry, cosmetics, etc. [25]. Poly(ethylene glycol) (PEG) hydrogels have been extensively employed in pharmaceutical applications and controlled drug release and provide stability for loaded protein drugs [26,27]. Moreover, Zn ions can coordinate with proteins and increase their stability during the formulation process [28,29]. Therefore, it is expected that a hydrogel consisting of γ-PGA, PEG, and Zn could be used as a reservoir for the sustained release of stabilized proteins. At present, Herceptin® is used for treating HER2-overexpressing breast cancer and metastatic gastric cancer and is administrated every 3 weeks through an IV or SC route. Therefore, an injectable hydrogel capable of high trastuzumab loading (>100 mg/mL) and the sustained release of trastuzumab could provide benefits of high local drug concentrations and sufficient systemic drug exposure for local and metastatic cancer treatments.

Herein, we developed novel chemically crosslinked hydrogels composed of γ-PGA-MA and 4-arm PEG-SH, which formed hydrogels through the thiol-maleimide reaction (Fig. 1). This highly negatively charged hydrogel was intended to carry high concentrations of trastuzumab (>100 mg/mL), and trastuzumab/Zn complexes should enhance the stability and retention of trastuzumab in the hydrogel. Rheological properties and morphologies of the hydrogels and the release behavior, structural integrity, and binding activity of trastuzumab released from these hydrogels were investigated. Furthermore, the antiproliferative effects of the released trastuzumab on human BT-474 breast cancer cells were studied to confirm the in vitro anticancer efficacy. Further, in vivo pharmacokinetic (PK) studies were performed to determine changes in plasma trastuzumab concentrations after being treated with a trastuzumab solution and the trastuzumab-loaded hydrogels. Finally, the in vivo antitumor efficacies of the various trastuzumab formulations were determined using a BT-474 xenograft tumor model.

2. Materials and methods

2.1. Materials

Herceptin® was purchased from Roche (Basel, Switzerland). γ-Polyglutamic acid sodium salt (γ-PGA-Na) (Mw 200–400 kDa) was purchased from Vedan (Taichung, Taiwan). *N*-(2-Aminoethyl) maleimide trifluoroacetate salt (AEM), *N*-hydroxysuccinimide (NHS), *N*-(3-dimethylaminopropyl)-*N*′-ethylcarbodiimide hydrochloride (EDC·HCl), and 3,3′,5,5′-tetramethylbenzidine (TMB) were purchased from Sigma-Aldrich (St. Louis, MO, USA). The 4-arm PEG-SH (Mn 5000) was purchased from SINOPEG (Xiamen, China). Zinc chloride was purchased from Alfa Aesar (Heysham, UK). All other chemicals were reagent grade and were used as received.

2.2. Synthesis of γ-PGA-MA

γ-PGA-Na (500 mg, 3.3 mmol) and AEM (500 mg, 2.0 mmol) were dissolved in 10 mL of deionized water. NHS (115 mg, 1.0 mmol) and EDC·HCl (190 mg, 1.0 mmol) were then sequentially added to the above solution. The reaction mixture was stirred at 1000 rpm for 48 h at room temperature. Thereafter, the solution was dialyzed (Spectra/Por MWCO 3500, Spectrum, USA) against 0.1 M acetate buffer of pH 5.0 for 2 days and then against deionized water for an additional 2 days. The solution was next filtered through a 0.22-μm filter and lyophilized. γ-PGA-MA was obtained as a pale yellow powder. The degree of substitution (DS) (carboxyl groups reacting with maleimide) was determined by ^{1}H nuclear magnetic resonance (NMR) spectroscopy (Varian 500 MHz NMR spectrometer, Varian, USA).

2.3. Preparation of trastuzumab-loaded hydrogels composed of γ-PGA-MA and 4-arm PEG-SH

Trastuzumab powder dissolved in deionized water was desalted, buffer exchanged, and concentrated to achieve the

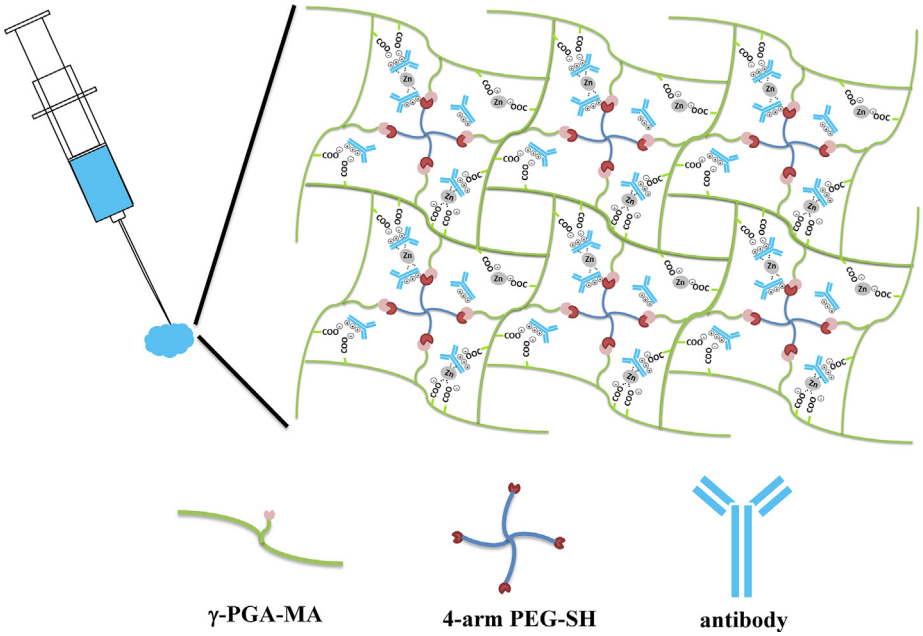

Fig. 1. Schematic illustration of a trastuzumab-loaded hydrogel composed of γ-poly glutamic acid (PGA)-maleimide (MA) and thiol end-functionalized 4-arm poly(ethylene glycol) (4-arm PEG-SH).

desired concentration of trastuzumab containing 0.9% NaCl by ultrafiltration using Spin-X® UF 30K MWCO Concentrators (Corning, USA). Proper amounts of γ-PGA-MA and 4-arm PEG-SH were dissolved in the trastuzumab solution to prepare trastuzumab-loaded hydrogel formulations with 1.5 wt% γ-PGA-MA and 1.5 wt % 4-arm PEG-SH. For trastuzumab/Zn-loaded hydrogels, an additional $ZnCl_2$ solution was added to the trastuzumab solution to achieve a final Zn concentration of 5 mM. The gelation time was determined by the tube inversion method, with 0.1 mL of the trastuzumab hydrogel formulation being loaded into a 1.5-mL centrifuge tube.

2.4. Morphologies of the hydrogels

The hydrogel formulation (0.1 mL) was loaded into a 1.5-mL centrifuge tube, and the hydrogel was allowed to form at room temperature. Then, the hydrogels were dried for 1 day using a lyophilizer (FTS Systems LyoStar II, Stone Ridge, NY, USA), and cross-sectional morphologies were observed using a scanning electron microscope (SEM) (JEOL JSM-5610LV, Tokyo, Japan) operated at 5 kV.

2.5. Rheological properties of the hydrogels

Rheological analysis of the hydrogel formulations was performed on a rotational rheometer (AR 2000ex, TA Instruments, UK) equipped with a 4-cm parallel plate. The hydrogel formulations were allowed to form at room temperature and then were transferred to a parallel plate of the rheometer. Measurements were conducted at 25 °C with a gap set to 1.0 mm. In the frequency sweep tests, the storage modulus (G′) and loss modulus (G″) of the hydrogels were recorded as a function of the frequency under 0.2% strain and a frequency of 1–100 rad/s. For the shear-shining tests, the viscosity was measured as a function of the shear rate at 0.1–10 s^{-1}. For the step strain tests, changes in G' and G″ were monitored under 0.2% strain for 200 s, with a sudden increase to 100% strain for 200 s, and then a return to 0.2% strain for subsequent 200 s; the frequency was set to 1 rad/s.

2.6. Trastuzumab assay and stability

The trastuzumab assay was performed at a wavelength of 280 nm with the reference wavelength at 340 nm using an Infinite® F200 PRO multimode plate reader (Tecan, Austria). The extinction coefficient of trastuzumab was 1.528 mL/(mg × cm) [30].

The monomer, high-molecular-weight species (HMWS), and low-molecular-weight species (LMWS) contents of trastuzumab were analyzed by size-exclusion high-performance liquid chromatography (SE-HPLC) using a Waters HPLC system (600 pump controller, 717 plus autosampler, and 996 photodiode array detector). A TSK Gel G3000 SWXL column (Tosoh Bioscience, Japan) with a TSK Gel SWXL 5 guard column (Tosoh Bioscience, Japan) was used. The mobile phase was composed of 0.05 M phosphate buffer and 0.15 M NaCl at pH 7.2. The SE-HPLC analysis was conducted at a flow rate of 0.5 mL/min, an injection volume of 100 μL, and a wavelength of 280 nm.

2.7. Zeta potential analysis of trastuzumab

The zeta potential of trastuzumab was measured with a Zetasizer Nano ZS (Malvern, UK). A trastuzumab solution of 5 mg/mL prepared in phosphate-buffered saline (PBS at pH 7.4) was transferred to a Disposable Capillary Cell (DTS1070), and measurements were performed at 25 °C. Data were collected and analyzed with Zetasizer software version 7.11.

2.8. Enzyme-linked immunosorbent assay (ELISA)

Nunc-Immuno™ MicroWell™ 96-well plates were coated with 100 μL of 0.4 μg/mL HER-2/ErB2 (Sino Biological, China). Freshly prepared trastuzumab and test samples of 10^{-7} M were threefold serially diluted and added to the plates for a 2-h incubation period at room temperature. After washing three times, the antihuman immunoglobulin G (IgG)-peroxidase Ab was added and incubated for 1 h at room temperature. Thereafter, the 96-well plates were washed, TMB was added for a 90-s incubation period, and then 1 M HCl was added. The absorbance was determined with an ELISA

reader (Thermo Labsystems, Finland) at 450 nm. The half-maximal binding concentration (EC_{50}) was calculated by sigmoidal fitting using Origin software 6.0 (MicroCal Software, Inc., USA).

2.9. In vitro cell antiproliferation

BT474 cells were seeded in a 96-well plate at a density of 8×10^3 cells/well in 100 μL of Dulbecco's modified Eagle medium (DMEM)/F12 medium (Thermo Fisher Scientific, USA) with 2% heat-inactivated fetal bovine serum. Then, 100 μL of various concentrations of either trastuzumab (freshly prepared trastuzumab solution or trastuzumab released from various hydrogels), $ZnCl_2$, or both was added and incubation for 90 h at 37 °C. Next, 22 μL of PrestoBlue™ Cell Viability Reagent (Invitrogen, USA) was added to each well and incubated for 4 h. The absorbance was analyzed with an Infinite® F200 PRO multimode plate reader (Tecan, Austria) at an excitation wavelength of 560 nm and emission wavelength of 590 nm. The dose-responsive curves for cell viability were generated by sigmoidal fitting using Origin software 6.0 (MicroCal Software, Inc., USA).

2.10. In vitro release of trastuzumab-loaded hydrogels

A trastuzumab hydrogel formulation (0.1 mL) was loaded into a 1.5-mL centrifuge tube, and 1.3 mL of release medium comprising 10 mM PBS (pH 7.4) was added. The tubes were placed in a shaking incubator at 37 °C and 100 rpm. At a predetermined time, 0.8 mL of release medium was sampled and replaced with fresh medium. The content, structural integrity, and binding affinity of the released trastuzumab were measured by UV detection, SE-HPLC, and ELISA, respectively. The mechanism of trastuzumab released from the hydrogel was investigated by fitting with various kinetic equations including zero-order, first-order, Higuchi, and Korsmeyer–Peppas models.

2.11. In vivo hydrogel formation

Sprague Dawley rats were purchased from BioLASCO Taiwan (Yilan, Taiwan). All experimental procedures for the animal studies were approved by the Institutional Animal Care and Use Committee of the Industrial Technology Research Institute (ITRI) (Hsinchu, Taiwan) (ITRI-IACUC-2017-011V3). Hydrogel formulations 400 μL were prepared and then subcutaneously injected into the shaved rats through a 23-gauge needle before gelation. After 14 days, the rats were sacrificed and the hydrogels wrapped in the rat skin and extracted from the skin were photographed.

2.12. In vivo pharmacokinetics

NOD SCID mice were purchased from BioLASCO Taiwan (Yilan, Taiwan) and divided into three groups ($n = 3$). All experimental procedures for the animal studies were approved by the Institutional Animal Care and Use Committee of the ITRI (Hsinchu, Taiwan) (ITRI-IACUC-2016-049 M). The trastuzumab solution group and trastuzumab hydrogel groups were treated with a subcutaneous injection of 10 mg/mL trastuzumab at a dose of 50 mg/kg. At predetermined time intervals, blood was obtained through a facial vein. Plasma was separated at 7000 rpm for 15 min and then stored at −80 °C until analysis. Trastuzumab concentrations were measured by a modified previously described ELISA method [31], and the limit of quantification was 0.06 μg/mL. PK parameters were calculated with a noncompartmental model using Phoenix WinNonlin 7.0 (Certara Inc., USA).

2.13. In vivo tumor inhibition

All experimental procedures for animal studies were approved by the Institutional Animal Care and Use Committees of ITRI (Hsinchu, Taiwan) (ITRI-IACUC-2016-045). BT474 cells (10^7 cells/mL) suspended in Matrigel (BD Biosciences, San Jose, CA, USA) were subcutaneously injected into the right flank of female NOD/SCID mice (BioLASCO, Taiwan) that were implanted with a 90-day-release 0.36-mg 17β-estradiol/pellet (Innovative Research of America, Sarasota, FL, USA). When the tumor volume reached 150–250 mm^3, the mice were randomly divided into five groups ($n = 6$): Group 1 mice were treated with PBS (5 mL/kg) as the control; group 2 mice received a blank hydrogel (5 mL/kg); group 3 mice were injected with a trastuzumab solution at a concentration of 10 mg/mL and dosing amount of 50 mg/kg (50 mg/5 mL/kg); group 4 mice were injected with Her-hydrogel-10 (50 mg/5 mL/kg); and group 5 mice were injected with Her/Zn-hydrogel-10 (50 mg/5 mL/kg). All mice received an SC injection on the back of the neck. The tumor volume was calculated as (length × $width^2$)/2. The change in the tumor volume of each group was monitored as a function of time. Moreover, the tumor growth inhibition (TGI) rate was calculated using the formula: [1 − (final tumor volume of treated group − initial tumor volume of treated group)/(final tumor volume of control group − initial tumor volume of control group)] × 100 [32]. Data are presented as mean ± standard deviation (SD).

2.14. Data analysis

Statistical analyses were performed with one-way analysis of variance (ANOVA) and Tukey's multiple comparison test, and differences were considered statistically significant at p values of <0.05.

3. Results and discussion

3.1. Synthesis of γ-PGA-MA

Maleimide-modified γ-PGA was obtained by reacting the carboxyl group of γ-PGA with the water-soluble AEM in the presence of EDC and NHS (Fig. 2A). As shown in the ^{1}H-NMR spectrum of γ-PGA-MA dissolved in D_2O (Fig. 2B), the D_2O signal was found at 4.7 ppm. This result indicated the successful synthesis of γ-PGA-MA with an additional proton signal of maleimide groups at 6.8 ppm compared to the ^{1}H-NMR spectrum of γ-PGA as reported in a previous study [33]. The DS of γ-PGA-MA was calculated on the basis of the integral ratio of the peak of two protons of maleimide at 6.8 ppm and the peak of proton CH of γ-GA at 4.1 ppm. The DS approximated to 10% by this synthesis process.

3.2. Characterization of trastuzumab-loaded hydrogel formulations

γ-PGA-MA and 4-arm PEG-SH formed a hydrogel through thiol-maleimide Michael-type addition reactions [34]. The molar ratio of thiol to maleimide was set to 1:1 to avoid chemical interactions between trastuzumab and excess functional maleimide groups or thiol groups. In addition, the trastuzumab-loaded γ-PGA-MA and 4-arm PEG-SH hydrogels prepared in a low ionic strength solution had an opalescence appearance owing to strong interactions between the positively charged trastuzumab (zeta potential of trastuzumab was 9.11 ± 0.78 mV) and negatively charged γ-PGA-MA. Therefore, 0.9% NaCl was used as a vehicle to obtain transparent trastuzumab-loaded hydrogels. Moreover, the rate of the Michael-type addition reaction is highly dependent on the pH and is much faster in alkaline conditions [35]. Therefore, the pH

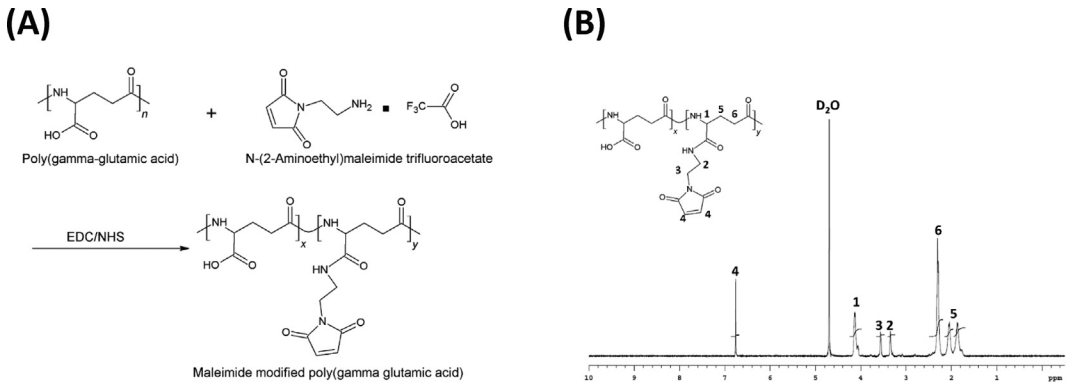

Fig. 2. (A) Synthesis of γ-PGA-MA. (B) ^{1}H NMR spectrum of γ-PGA-MA.

of the hydrogel formulations was controlled to below 6.5 to obtain uniform hydrogels.

Table 1 lists 1.5% γ-PGA-MA- and 1.5% 4-arm PEG-SH-based hydrogel compositions. The blank hydrogel with a pH value of 5.0 gelled at 35–40 min, and the gelation time was a little delayed in the presence of 5 mM $ZnCl_2$, which led to a more acidic condition (ca. pH 4.5) of the hydrogel formulation. When 10 or 133 mg/mL of trastuzumab was loaded into the hydrogel composition (Her-hydrogel-10, Her/Zn-hydrogel-10, Her-hydrogel-133, and Her/Zn-hydrogel-133), the pH of the formulation increased to ca. 6.0. Compared to the blank hydrogel or blank Zn-hydrogel, all trastuzumab-loaded hydrogels had faster gelling rates, and gelation times decreased with increased trastuzumab loading. This indicates that the electrostatic attraction between trastuzumab and γ-PGA-MA and the pH of the reaction environment affected gelation times. In addition, compared to Her-hydrogels, Her/Zn-hydrogels had longer gelation times, which was attributed to the formation of trastuzumab/Zn nanocomplexes that reduced the electrostatic attraction between trastuzumab and γ-PGA-MA. Most importantly, high trastuzumab loading (>100 mg/mL) was achievable as demonstrated by the formation of Her-hydrogel-133 and Her/Zn-hydrogel-133.

3.3. Morphologies of trastuzumab-loaded hydrogel formulations

Microstructures of hydrogels composed of γ-PGA-MA and 4-arm PEG-SH were investigated by SEM. According to the cross-sectional SEM images of hydrogels (Fig. 3), all hydrogel formulations possessed porous microstructures, thus indicating that these hydrogels had been formed through cross-linking between maleimide groups and thiol groups. In addition, the porosity of the hydrogels appeared to vary with the additives. Compared to blank hydrogels, homogeneous and smaller pores of ca. 50 μm in diameter were observed in the blank Zn-hydrogels (Fig. 3A vs. B). This phenomenon was ascribed to electrostatic interactions between carboxyl groups of γ-PGA-MA and Zn ions. Furthermore, hydrogels loaded with trastuzumab had more compact microstructures with pore sizes of 10–50 μm (Fig. 3C, D), thus indicating that electrostatic interactions had occurred between carboxyl groups of γ-PGA-MA and trastuzumab.

3.4. Rheological properties of trastuzumab-loaded hydrogel formulations

Rheological properties of hydrogels composed of γ-PGA-MA and 4-arm PEG-SH were investigated by a frequency sweep test, flow sweep test, and dynamic step strain amplitude test, and data are shown in Fig. 4. As shown in Fig. 4A and D, blank hydrogels composed of 1.5% γ-PGA-MA and 1.5% 4-arm PEG-SH had a storage modulus, G', of ~650 Pa. The addition of 5 mM $ZnCl_2$ into the above hydrogel caused a 30% increase in the G′ value (~850 vs. ~650 Pa) due to electrostatic interactions of Zn ions coordinating with carboxyl groups of γ-PGA-MA chains. Her-hydrogel-10 composed of 1.5% γ-PGA-MA, 1.5% 4-arm PEG-SH, and 10 mg/mL trastuzumab had a higher G′ value than the blank hydrogel (~770 vs. ~650 Pa). It is thought that electrostatic interactions between cationic trastuzumab and anionic γ-PGA-MA could result in greater interchain attraction, correspondingly increasing the gel strength (G′ value). On the other hand, Her/Zn-hydrogel-10 composed of 1.5% γ-PGA-MA, 1.5% 4-arm PEG-SH, 5 mM $ZnCl_2$, and 10 mg/mL trastuzumab had a lower G' value than the blank Zn hydrogel (~760 vs. ~850 Pa). This was attributed to possible electrostatic interactions between trastuzumab and Zn ions, which resulted in interactions between γ-PGA-MA and either trastuzumab or Zn ions being minimized, thus leading to lower gel strengths. On the basis of the above data, hydrogel strength primarily depended on the network formed upon thiol-maleimide interactions and only slightly changed with the addition of either trastuzumab, Zn ions, or both.

The decrease in viscosity of all hydrogel formulations with an increasing shear rate is shown in Fig. 4B and E, thus indicating that these hydrogel formulations had shear-thinning properties.

Table 1
Compositions of γ-PGA-MA and 4-arm PEG-SH hydrogel formulations.

Formula	Trastuzumab (mg/mL)	$ZnCl_2$ (mM)	γ-PGA-MA		4-arm PEG_{5K}-SH (wt, %)	SH/MA molar ratio	G′ (Pa)	Gelation time (min)
			wt (%)	DS (%)				
Blank hydrogel	0	0	1.5	11.5	1.5	1	~650	35–40
Blank Zn-hydrogel	0	5	1.5	11.5	1.5	1	~800	45–50
Her-hydrogel-10	10	0	1.5	11.5	1.5	1	~770	30–35
Her/Zn-hydrogel-10	10	5	1.5	11.5	1.5	1	~760	40–45
Her-hydrogel-133	133	0	1.5	10.5	1.5	1	–	5–10
Her/Zn-hydrogel-133	133	5	1.5	10.5	1.5	1	–	20–25

DS, degree of substitution; G', storage modulus.

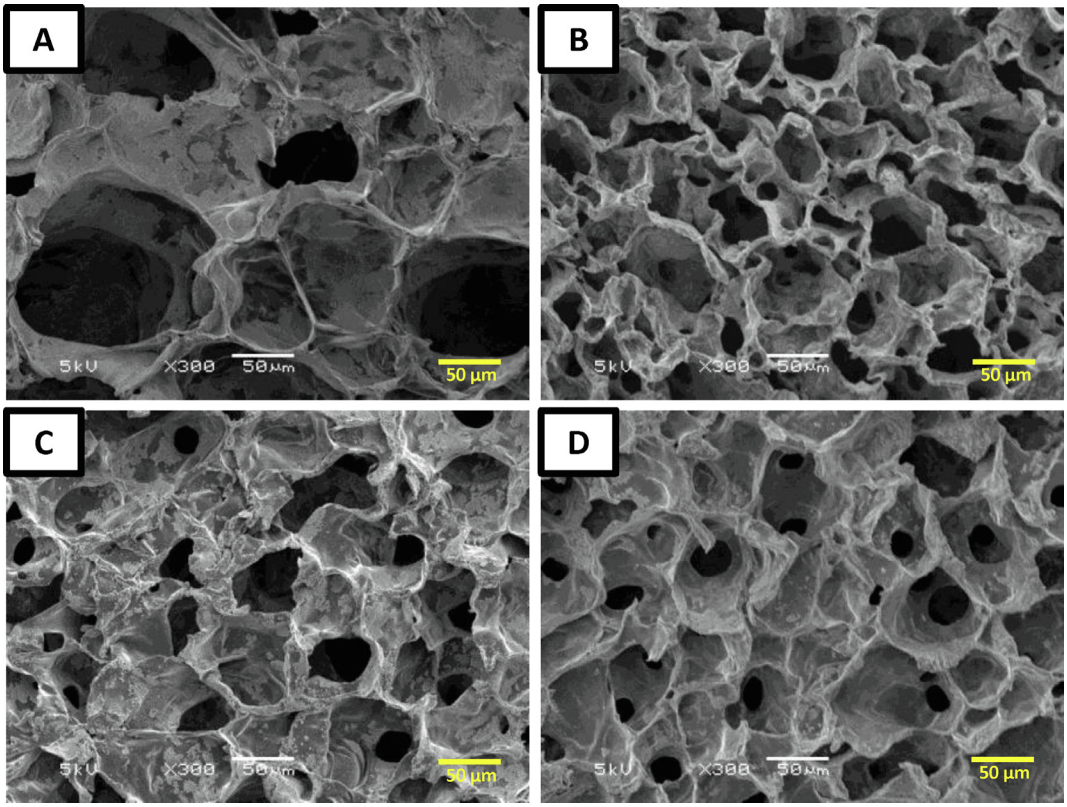

Fig. 3. SEM images of hydrogels composed of 1.5% γ-PGA-MA and 1.5% 4-arm PEG-SH. (A) Blank hydrogel. (B) Blank Zn hydrogel. (C) Her-hydrogel-10. (D) Her/Zn-hydrogel-10.

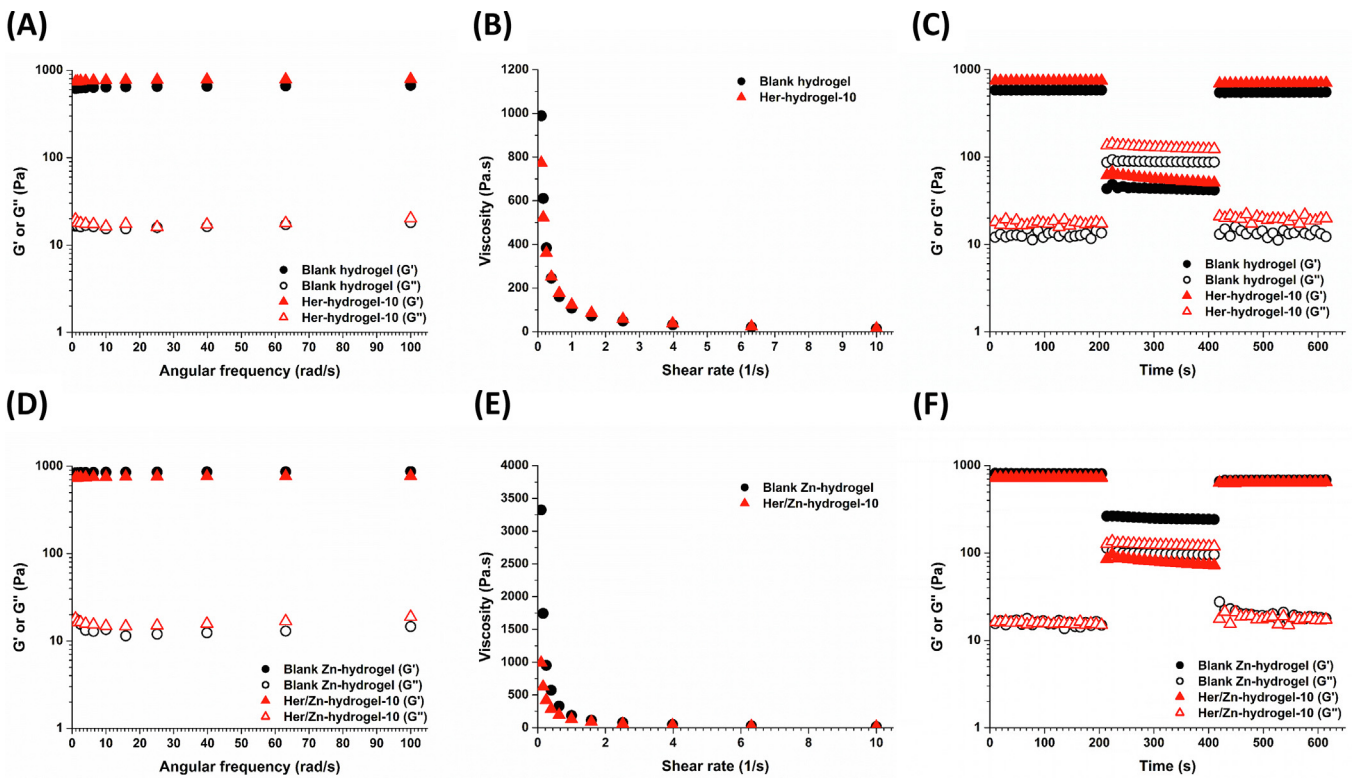

Fig. 4. Frequency sweep, flow sweep, and dynamic step strain amplitude tests of a blank hydrogel and a Her-hydrogel-10 (A–C) and a blank Zn-hydrogel and a Her/Zn-hydrogel-10 (D–F).

Moreover, a dynamic step strain amplitude test was performed to determine the recovery of hydrogels undergoing network rupture under a high strain condition (γ = 100%), followed by low strain (γ = 0.2%). Fig. 4C and F demonstrate that G′ values of the blank hydrogel, Her-hydrogel-10, blank Zn-hydrogel, and Her/Zn-hydrogel-10 significantly decreased by 13-, 13.5-, 3-, and 9-fold, respectively, when subjected to high strain. When the condition changed to low strain, G′ values of all hydrogel formulations recovered within seconds, with a loss of <10%. Further, G′ values of all hydrogel formulations were higher than G″ values at low strain (γ = 0.2%), and inverse results were observed at high strain (γ = 100%) except for the blank Zn-hydrogel. The electrostatic attraction between Zn ions and γ-PGA-MA enhanced the mechanical properties of the blank Zn-hydrogel, and hence, it could remain as a gel state at high strain. Compared to the blank Zn-hydrogel, the apparent decrease in the G′ value of the Her/Zn-hydrogel-10 in a high-strain condition hinted that Zn ions were still interacting with trastuzumab in the presence of γ-PGA-MA, and then interactions of Zn ions with γ-PGA-MA were reduced in Her/Zn-hydrogel-10. Rheological studies indicated that hydrogel formulations could rapidly form a gel after removing the shear force and could serve as an injectable hydrogel for the sustained release of desired active substances.

3.5. In vitro release behaviors and stability of trastuzumab from hydrogel formulations

The in vitro release behaviors of trastuzumab-loaded hydrogels were investigated by immersing the hydrogels in PBS (pH 7.4) at 37 °C. SE-HPLC analysis and ELISA assay were used to confirm the structural integrity and binding activity of the released trastuzumab, respectively. Fig. 5 shows cumulative release profiles of trastuzumab-loaded hydrogels. Her-hydrogel-10 and Her/Zn-hydrogel-10 were capable of continually releasing trastuzumab over 4 weeks with a burst release (release on day 1) of ca. 10%–13%. Moreover, Her-hydrogel-133 and Her/Zn-hydrogel-133 demonstrated sustained release of trastuzumab over 5–7 weeks with an initial burst release of ca. 7%–10%. Owing to the hydrodynamic radius of trastuzumab (Rh ~5.4 nm) [36], which is much smaller than the pore size of the hydrogels (10–50 μm), the sustained-release mechanism of trastuzumab from polyanionic hydrogels was mainly diffusion dependent under the influence of electrostatic interactions [23,24]. These results indicated that increasing trastuzumab loading or adding Zn to the hydrogel formulations could enhance interactions between trastuzumab molecules or form trastuzumab/Zn nanocomplexes, thus leading to the retardation of trastuzumab release from the hydrogels.

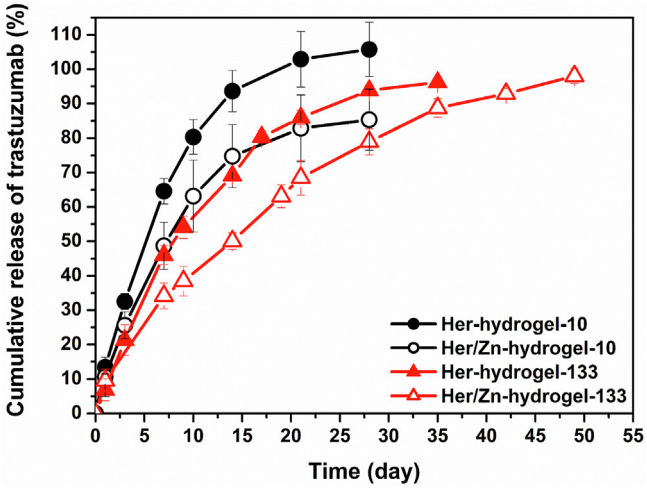

Fig. 5. Cumulative release of trastuzumab from various trastuzumab-loaded hydrogels at 37 °C.

The mechanism of trastuzumab released from the hydrogel was investigated by fitting with various kinetic equations including zero-order, first-order, Higuchi, and Korsmeyer–Peppas models (Table 2). The high correlation in the first-order and Higuchi models for all trastuzumab hydrogel formulations was obtained with a linear regression coefficient (R^2) of >0.95, thus indicating a concentration and diffusion-dominated release behavior. Furthermore, the release exponent value (Korsmeyer-Peppas model) of these hydrogel formulations was ranging from 0.6099 to 0.7499, thus indicating a non-Fickian release profile [37]. Therefore, the trastuzumab released from this hydrogel was governed by a combination of diffusion and swelling. We also found that all hydrogel formulations swelled up to ca. 30% of their size after the dissolution studies. Fig. S1 showed the SEM data of the Her/Zn-hydrogel-10 before and after 28 days of dissolution study. After dissolution study, the pore size of the Her/Zn-hydrogel-10 was apparently increasing, thus indicating that swelling occurred.

Table 3 shows percentage changes of the trastuzumab monomer and EC_{50} values of trastuzumab released during the dissolution study. Her-hydrogel-10 liberated trastuzumab as a monomer (>99.5%) and maintained the binding activity of trastuzumab over 21 days of dissolution. Moreover, the monomer content of trastuzumab released from Her-hydrogel-133 exceeded 95% and exhibited a comparable binding affinity to freshly prepared trastuzumab. For Her/Zn-hydrogel-10 and Her/Zn-hydrogel-133, approximately 3% and 30% of HMWS were observed in PBS, respectively, thereby resulting from interactions between Zn ions and trastuzumab [28], and these water-soluble aggregations of trastuzumab could further transform into a monomer, as it was diluted in the histidine solution (Fig. S2), thus indicating that trastuzumab-Zn coordination complexes were not irreversible but reversible aggregations. Importantly, Her/Zn-hydrogel-10 and Her/Zn-hydrogel-133 also preserved the intact binding activity of trastuzumab during the release period. The above results suggest that trastuzumab still maintained its structural integrity and intact

Table 2
In vitro release modeling of various trastuzumab formulations.

Formula	Zero order $C_t = C_0 + K_0t$	First order Log C_r = Log $C_0 - k_1t/2.303$	Higuchi $Q = K_Ht^{1/2}$	Korsmeyer–Peppas $M_t/M_\infty = K_{kp}t^n$	
	R^2	R^2	R^2	n	R^2
Her-hydrogel-10	0.8202	0.9782	0.9586	0.6424	0.9592
Her/Zn-hydrogel-10	0.8385	0.9553	0.9651	0.6492	0.9668
Her-hydrogel-133	0.8638	0.9963	0.9723	0.7499	0.9611
Her/Zn-hydrogel-133	0.9145	0.9573	0.9925	0.6099	0.9948

C_t, amount of drug released at time t; C_0, initial concentration of drug at time t = 0; K_0, zero-order rate constant; t, time; C_r, remaining drug at time t; K_1, first-order rate constant; Q, cumulative amount of drug released at time t; K_H, Higuchi dissolution rate constant; M_t/M_∞, fraction of drug released at time t; K_{kp}, Korsmeyer release rate constant; n, drug release exponent.

Table 3
Monomer percentage and the half maximal binding concentration (EC_{50}) of released trastuzumab after the dissolution study.

	Her-hydrogel-10		Her/Zn-hydrogel-10		Her-hydrogel-133		Her/Zn-hydrogel-133	
	Monomer (%)	EC_{50} (nM)	Monomer (%)	EC_{50} (nM)	Monomer (%)	EC_{50} (nM)	Monomer (%)	EC_{50} (nM)
Day 1	100.0 ± 0.0	–	100.0 ± 0.0	–	99.9 ± 0.1	–	96.8 ± 0.9 (100.0 ± 0.0)[b]	–
Day 7	100.0 ± 0.0	0.47 (0.50)[b]	100.0 ± 0.0	0.50 (0.50)[b]	100.0 ± 0.0	0.50 (0.57)[b]	77.8 ± 3.2 (100.0 ± 0.0)[c]	0.64 (0.57)[b]
Day 14[a]	100.0 ± 0.0	0.49 (0.60)[b]	96.5 ± 0.4 (100.0 ± 0.0)[c]	0.55 (0.60)[b]	100.0 ± 0.0	0.87 (0.78)[b]	67.9 ± 2.9 (100.0 ± 0.0)[c]	0.69 (0.57)[b]
Day 21	100.0 ± 0.0	–	97.2 ± 1.4 (100.0 ± 0.0)[c]	0.48 (0.60)[b]	98.8 ± 0.9	0.81 (0.73)[b]	68.8 ± 4.0 (98.8 ± 1.0)[c]	0.86 (0.78)[b]
Day 28	–	–	–	–	98.2 ± 1.0	0.90 (0.73)[b]	76.6 ± 8.9 (97.0 ± 2.9)[c]	0.73 (0.53)[b]
Day 35	–	–	–	–	95.6 ± 5.3	1.01 (0.73)[b]	71.1 ± 7.1 (96.6 ± 2.3)[c]	0.79 (0.53)[b]
Day 42	–	–	–	–	–	–	77.9 ± 4.8 (94.8 ± 3.0)[c]	0.79 (0.53)[b]

[a] The monomer percentage is presented as mean ± standard deviation ($n = 3$).
[b] EC_{50} of freshly prepared trastuzumab.
[c] Monomer percentage of the released trastuzumab after dilution in a histidine HCl solution.

binding activity during the thiol-maleimide crosslinking reactions and the release period.

3.6. Antiproliferative effects of trastuzumab released from hydrogel formulations on BT-474 cells

The Her2-overexpressing BT-474 breast cancer cell line was used to confirm the in vitro anticancer efficacy of trastuzumab released from the hydrogel formulations. As shown in Fig. 6A–D, after 90 h of treatment with the trastuzumab solution, the viability of BT474 cells remained at ca. 60% as the trastuzumab concentration was >1.0 μg/mL. The observed data indicated that exceeding the effective therapeutic dose would not further increase cytotoxicity and were comparable to that of previous studies [11]. Furthermore, the trastuzumab released from Her-hydrogel-10 (14 days of dissolution), Her/Zn-hydrogel-10 (14 days of dissolution), Her-hydrogel-133 (21 days of dissolution), and Her/Zn-hydrogel-133 (21 days of dissolution) exhibited similar antiproliferative effects on BT-474 cells compared to freshly prepared trastuzumab. On the other hand, BT-474 cells treated with Zn also exhibited a dose-dependent growth inhibitory effect at Zn concentrations ranging from 2.5 to 20 μg/mL, the almost complete suppression of cell growth with >20 μg/mL Zn, and a minimum effect on cell viability with <2.5 μg/mL Zn (Fig. 6E). Therefore, various concentrations of trastuzumab accompanied by 2.5 μg/mL Zn were used to examine the synergistic effects of Zn and trastuzumab on BT-474 cells. The data indicated that the combination of Zn and trastuzumab had similar cell growth inhibitory effects as those of trastuzumab alone (Fig. 6F). The above results suggested that trastuzumab released from these hydrogel formulations maintained a sufficient inhibitory ability against BT-474 cells, and only Zn concentrations of >2.5 μg/mL played a role in growth inhibition of BT-474 cells.

3.7. In vivo hydrogel formation

The in vivo hydrogel formation was confirmed by administering a subcutaneous injection of the blank Zn-hydrogel formulation (before gelation) into a Sprague Dawley rat. After 14 days, the hydrogel could be found at the injection site (Fig. S3A). Additionally, the hydrogel could be extracted and sliced into half (Fig. S3B). These data indicated that the γ-PGA-MA and 4-arm PEG-SH-based formulation could form a hydrogel in situ and maintain as a gel type for at least 14 days.

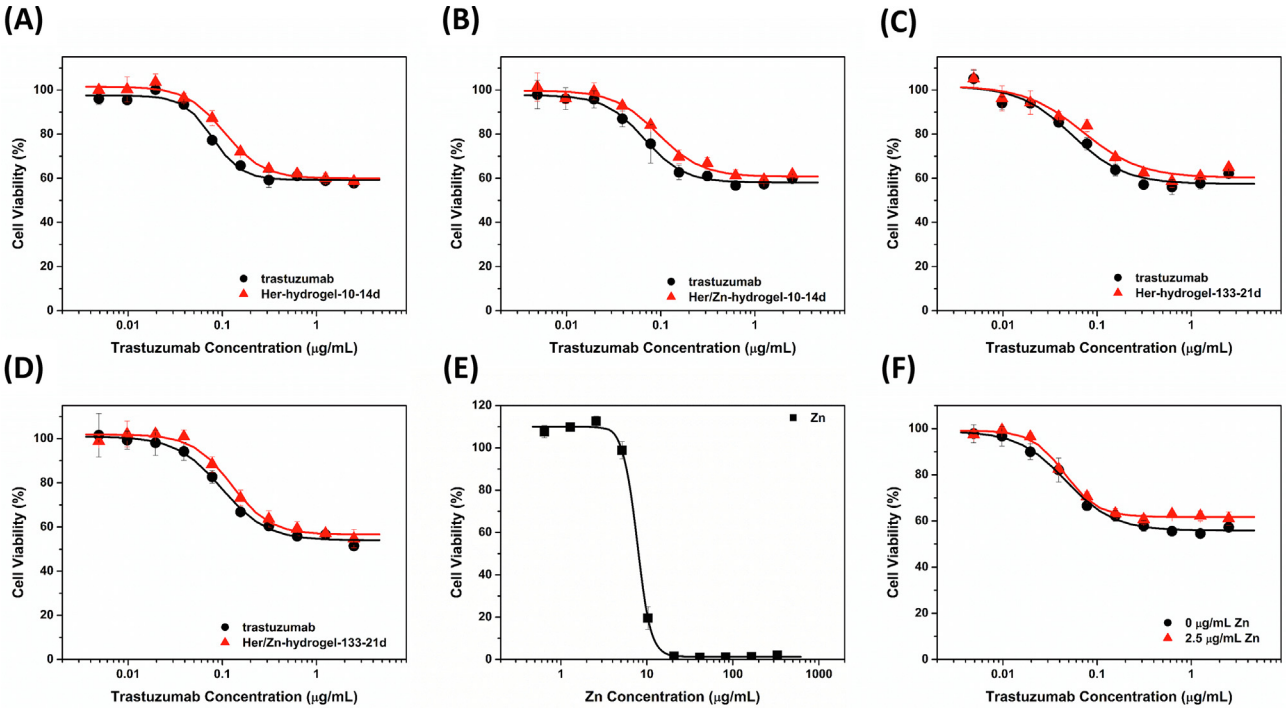

Fig. 6. Viability of BT-474 cells after 90 h of treatment with various concentrations of either trastuzumab, $ZnCl_2$, or both. (A) Her-hydrogel-10 at 14 days, (B) Her/Zn-hydrogel-10 at 14 days, (C) Her-hydrogel-133 at 21 days, (D) Her/Zn-hydrogel-133 at 21 days, (E) $ZnCl_2$, and (F) a combination of trastuzumab and $ZnCl_2$.

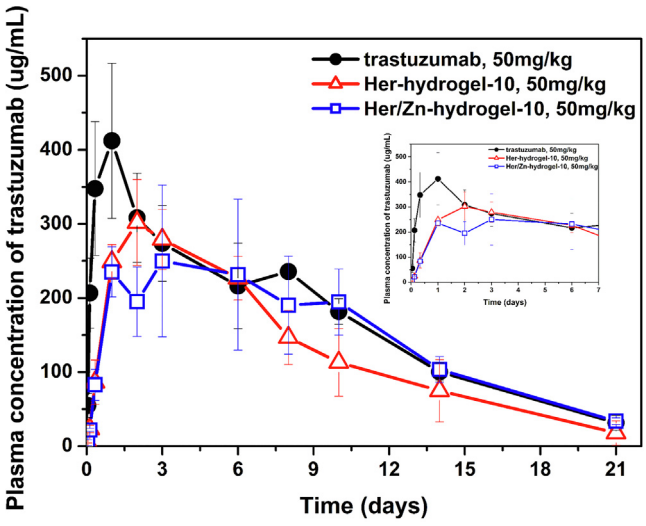

Fig. 7. Pharmacokinetic profiles of trastuzumab formulations in NOD SCID mice at a dose of 50 mg/kg.

3.8. In vivo PK of trastuzumab-loaded hydrogel formulations

In vivo PK studies of various trastuzumab formulations were performed in NOD SCID mice at a dose of 50 mg/kg, and PK parameters including $T_{1/2}$, C_{max}, T_{max}, and the area under the plasma drug concentration–time curve (AUC) were evaluated. In vivo PK profiles of the trastuzumab formulations are presented in Fig. 7, and related PK parameters are listed in Table 4. After SC administration of the trastuzumab solution, a C_{max} of 362–532 μg/mL was observed on days 1–2, and then, the trastuzumab concentration gradually decreased as time progressed. On the contrary, Her-hydrogel-10 and Her/Zn-hydrogel-10 had much lower trastuzumab exposure (ca. <60% of the trastuzumab solution) on day 1 than the trastuzumab solution, thus indicating that γ-PGA-MA- and 4-arm PEG-SH-based hydrogels had the ability to reduce the initial diffusion rate of trastuzumab in the SC region. Thereafter, both hydrogels could achieve similar trastuzumab concentrations as those of the trastuzumab solution after day 6. The obtained PK characteristics were similar to those of previous studies using a polyanionic hydrogel to deliver mAbs subcutaneously in rodents [12,23]. Further, compared to Her-hydrogel-10, Her/Zn-hydrogel-10 provided a constant trastuzumab concentration for 10 days, which demonstrated that Her/Zn-hydrogel-10 possessed a better sustained release ability of trastuzumab than Her-hydrogel-10 owing to the presence of trastuzumab/Zn nanocomplexes that retarded the release rate of trastuzumab from the hydrogel. These data correlated well with the in vitro release study results. In addition, the relative bioavailabilities (versus the trastuzumab solution) of Her-hydrogel-10 and Her/Zn-hydrogel-10 were 77% and 88%, respectively, thus indicating that sufficient trastuzumab could be released from the hydrogels. In this study, the injection volume of hydrogels was approximately 100 μL, and it is expected that sustained release PK profiles could be better as the injection volume increased. PK results indicated that the hydrogel formulations had the ability to demonstrate sustained release of trastuzumab and could provide sufficient systemic exposure to trastuzumab.

Table 4
Pharmacokinetic parameters of trastuzumab formulations in NOD SCID mice at a dose of 50 mg/kg.[a]

	Trastuzumab solution	Her-hydrogel-10	Her/Zn-hydrogel-10
T_{max} (days)	1.3 ± 0.6	1.7 ± 0.6	2.7 ± 2.9
C_{max} (μg/mL)	423.9 ± 94.3	307.1 ± 49.3	279.4 ± 59.3
$AUC_{0\text{-}21d}$ (μg/mL*day)	3604.1 ± 198.4	2783.1 ± 601.2	3160.6 ± 845.2

$T_{1/2}$, terminal half-life; T_{max}, time to reach the C_{max}; C_{max}, maximum plasma concentration of trastuzumab; $AUC_{0\text{-}21d}$, area under the curve of plasma concentration of trastuzumab versus time on days 0–21.

[a] Data are presented as mean ± standard deviation (n = 3).

3.9. Antitumor efficacies of trastuzumab-loaded hydrogel formulations in the BT-474 xenograft tumor model

The in vivo antitumor efficacies of the trastuzumab formulations were evaluated in a BT-474 xenograft tumor model. Changes in the tumor volume as a function of time were recorded after SC administration of PBS, blank hydrogel, trastuzumab solution, Her-hydrogel-10, and Her/Zn-hydrogel-10 at a dose of 50 mg/kg trastuzumab. Fig. 8A exhibits the antitumor efficacies of various formulations, and the ANOVA detected statistically significant differences among groups ($p < 0.001$). Furthermore, Tukey's test showed that mice treated with the blank hydrogel exhibited no effect on tumor inhibition compared to the mice in the PBS group ($p > 0.05$). This implied that the γ-PGA-MA- and 4-arm PEG-SH-based hydrogels did not cause any cytotoxic effect on the tumors. For mice treated with trastuzumab or Her-hydrogel-10, slight tumor inhibition was observed with respective TGI values of 51.0% ± 37.9% and 52.2% ± 51.4% on day 28 after treatment. However, tumor sizes of mice in the trastuzumab group and Her-hydrogel-10 group did not show significant difference compared

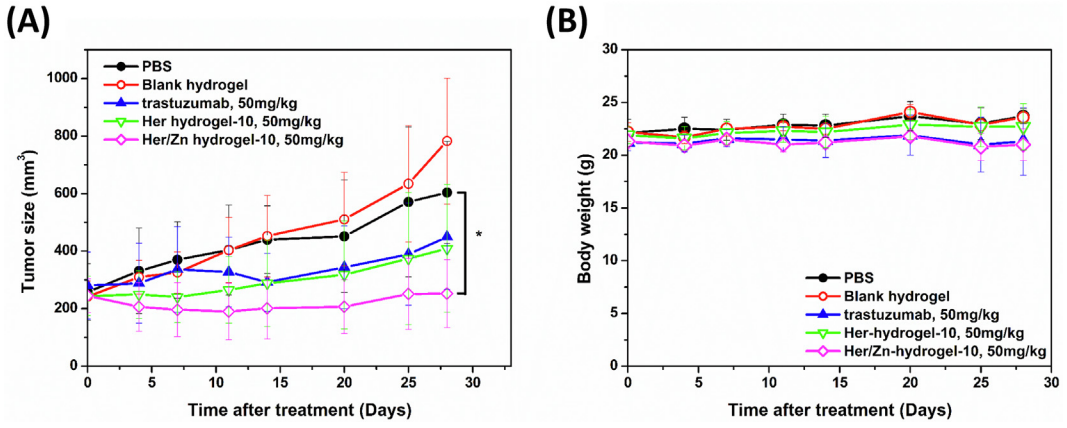

Fig. 8. (A) Antitumor efficacy and (B) body weight changes in BT474-tumor bearing mice after treatment with trastuzumab formulations (n = 6). *The tumor size of the Her/Zn-hydrogel-10 group showed significant difference compared to that of the phosphate-buffered saline (PBS) group ($p < 0.05$).

to those of mice in the PBS group ($p > 0.05$). These results were not in acceptable agreement with those given in recent reports [10–12]. Injectable hydrogel with sustained release ability of mAb had advantages of preventing rapid degradation of mAb and increasing the mAb accumulation at the tumor site, and it might lead to better antitumor efficacy than solution formulations [10–12]. Further, antitumor mechanism based on trastuzumab-induced dose-dependent apoptosis was effective at a dose of 30 mg/kg [11,12]. Interestingly, mice treated with Her/Zn-hydrogel-10 exhibited an unexpected tumor inhibitory effect over 4 weeks with a TGI of 97.8% ± 31.7% on day 28 after treatment, and the tumor size of mice in this group was much smaller than that of mice in the PBS group after 28 days ($p < 0.05$). As mentioned in the BT-474 antiproliferation and PK results, the viability of BT-474 cells remained at ca. 60% when the trastuzumab concentration was >1.0 μg/mL, and comparable trastuzumab concentrations were observed with various trastuzumab formulations 7 days after dosing. On the basis of PK results, we expected that similar antitumor efficacies would occur with the trastuzumab solution and hydrogel formulations owing to the injection site being located 4–5 cm distant from the tumor site. Consequently, the better antitumor effect in the Her/Zn-hydrogel-10 group could possibly be attributed to the functionality of Zn, which showed the potential for growth inhibition in several cancer cell lines [38,39]. Further, the viability of BT-474 cells treated with Zn (Fig. 6E) indicated that Zn might play a role in enhancing the anticancer effect of the Her/Zn-hydrogel group. In addition, Fig. 8B demonstrates that no apparent changes in body weight occurred in any treatment groups.

4. Conclusions

In this work, injectable hydrogels composed of γ-PGA-MA and 4-arm PEG-SH were developed for the SC delivery of trastuzumab. Through thiol-maleimide reactions, γ-PGA-MA and 4-arm PEG-SH formed a hydrogel with shear-thinning properties and reversible rheological behavior. This novel hydrogel was capable of loading a high content of trastuzumab (>100 mg/mL) and showing a sustained release of trastuzumab over several weeks. In addition, the trastuzumab released from the hydrogel maintained its structural integrity, binding bioactivity, and BT-474 cell antiproliferative effect. PK studies demonstrated that trastuzumab hydrogels could lower the C_{max} and achieve similar trastuzumab concentrations on day 6 after dosing than that of the trastuzumab solution. An in vivo antitumor investigation indicated that trastuzumab hydrogels had similar tumor growth-inhibitory effects as those of the trastuzumab solution. On the other hand, Zn-containing trastuzumab hydrogels exhibited a superior capability of tumor growth inhibition ascribed to the functionality of Zn. Consequently, these results implied that γ-PGA-MA- and 4-arm PEG-SH-based hydrogels have great potential to serve as carriers for local or systemic delivery of therapeutic proteins and antibodies.

Acknowledgments

This work was supported by the Ministry of Economic Affairs, Taiwan, and Taipei Medical University, Taiwan. Ms. Tzu-Tung Yu from JHL Biotech, Inc., is acknowledged for the in vitro activity determination.

Conflict of interest

The authors declare financial interests with a patent application.

Appendix A. Supplementary data

Supplementary data to this article can be found online at https://doi.org/10.1016/j.actbio.2019.01.003.

References

[1] D.M. Ecker, S.D. Jones, H.L. Levine, The therapeutic monoclonal antibody market, mAbs 7 (1) (2014) 9–14.
[2] J.M. Reichert, Antibodies to watch in 2017, MAbs 9 (2) (2017) 167–181.
[3] L.H. Bookbinder, A. Hofer, M.F. Haller, M.L. Zepeda, G.A. Keller, J.E. Lim, T.S. Edgington, H.M. Shepard, J.S. Patton, G.I. Frost, A recombinant human enzyme for enhanced interstitial transport of therapeutics, J. Control. Release 114 (2) (2006) 230–241.
[4] C. Aalbers, D. Gerlag, K. Vos, M. Vervoordeldonk, R. Landewe, P.P. Tak, Intra-articular etanercept treatment in inflammatory arthritis: a randomized double-blind placebo-controlled proof of mechanism clinical trial validating TNF as a potential therapeutic target for local treatment, Joint Bone Spine 82 (5) (2015) 338–344.
[5] F. Conti, R. Priori, M.S. Chimenti, G. Coari, A. Annovazzi, G. Valesini, A. Signore, Successful treatment with intraarticular infliximab for resistant knee monarthritis in a patient with spondylarthropathy: a role for scintigraphy with 99mTc-infliximab, Arthritis Rheumatol. 52 (4) (2005) 1224–1226.
[6] J.M. Korth-Bradley, A.S. Rubin, R.K. Hanna, D.K. Simcoe, M.E. Lebsack, The pharmacokinetics of etanercept in healthy volunteers, Ann. Pharmacother. 34 (2) (2000) 161–164.
[7] P. Adamson, T. Wilde, E. Dobrzynski, C. Sychterz, R. Polsky, E. Kurali, R. Haworth, C.M. Tang, J. Korczynska, F. Cook, I. Papanicolaou, L. Tsikna, C. Roberts, Z. Hughes-Thomas, J. Walford, D. Gibson, J. Warrack, J. Smal, R. Verrijk, P.E. Miller, T.M. Nork, J. Prusakiewicz, T. Streit, S. Sorden, C. Struble, B. Christian, I.R. Catchpole, Single ocular injection of a sustained-release anti-VEGF delivers 6months pharmacokinetics and efficacy in a primate laser CNV model, J. Control. Release 244 (Pt A) (2016) 1–13.
[8] L.R. Asmus, J.P. Grimshaw, P. Richle, B. Eicher, D.M. Urech, R. Gurny, M. Moller, Injectable formulations for an intravitreal sustained-release application of a novel single-chain VEGF antibody fragment, Eur. J. Pharm. Biopharm. 95 (Pt B) (2015) 250–260.
[9] M.L. Lovett, X. Wang, T. Yucel, L. York, M. Keirstead, L. Haggerty, D.L. Kaplan, Silk hydrogels for sustained ocular delivery of anti-vascular endothelial growth factor (anti-VEGF) therapeutics, Eur. J. Pharm. Biopharm. 95 (Pt B) (2015) 271–278.
[10] A.L. Lee, V.W. Ng, S. Gao, J.L. Hedrick, Y.Y. Yang, Injectable biodegradable hydrogels from vitamin D-functionalized polycarbonates for the delivery of avastin with enhanced therapeutic efficiency against metastatic colorectal cancer, Biomacromolecules 16 (2) (2015) 465–475.
[11] A.L.Z. Lee, V.W.L. Ng, S. Gao, J.L. Hedrick, Y.Y. Yang, Injectable hydrogels from triblock copolymers of vitamin E-functionalized polycarbonate and poly (ethylene glycol) for subcutaneous delivery of antibodies for cancer therapy, Adv. Funct. Mater. 24 (11) (2014) 1538–1550.
[12] K. Xu, F. Lee, S. Gao, M.H. Tan, M. Kurisawa, Hyaluronidase-incorporated hyaluronic acid-tyramine hydrogels for the sustained release of trastuzumab, J. Control. Release 216 (2015) 47–55.
[13] T.C. Gangadhar, R.H. Vonderheide, Mitigating the toxic effects of anticancer immunotherapy, Nat. Rev. Clin. Oncol. 11 (2) (2014) 91–99.
[14] M.F. Fransen, F. Ossendorp, R. Arens, C.J. Melief, Local immunomodulation for cancer therapy: providing treatment where needed, Oncoimmunology 2 (11) (2013) e26493.
[15] M.F. Fransen, T.C. van der Sluis, F. Ossendorp, R. Arens, C.J. Melief, Controlled local delivery of CTLA-4 blocking antibody induces CD8+ T-cell-dependent tumor eradication and decreases risk of toxic side effects, Clin. Cancer Res. 19 (19) (2013) 5381–5389.
[16] S. Rahimian, M.F. Fransen, J.W. Kleinovink, M. Amidi, F. Ossendorp, W.E. Hennink, Polymeric microparticles for sustained and local delivery of antiCD40 and antiCTLA-4 in immunotherapy of cancer, Biomaterials 61 (2015) 33–40.
[17] R.J. Harris, S.J. Shire, C. Winter, Commercial manufacturing scale formulation and analytical characterization of therapeutic recombinant antibodies, Drug Dev. Res. 61 (3) (2004) 137–154.
[18] D.F. Martin, M.G. Maguire, S.L. Fine, G.S. Ying, G.J. Jaffe, J.E. Grunwald, C. Toth, M. Redford, F.L. Ferris 3rd, Ranibizumab and bevacizumab for treatment of neovascular age-related macular degeneration: two-year results, Ophthalmology 119 (7) (2012) 1388–1398.
[19] J. Zhao, X. Zhao, B. Guo, P.X. Ma, Multifunctional interpenetrating polymer network hydrogels based on methacrylated alginate for the delivery of small molecule drugs and sustained release of protein, Biomacromolecules 15 (9) (2014) 3246–3252.
[20] J. Qu, X. Zhao, P.X. Ma, B. Guo, pH-responsive self-healing injectable hydrogel based on N-carboxyethyl chitosan for hepatocellular carcinoma therapy, Acta Biomater. 58 (2017) 168–180.
[21] J. Qu, X. Zhao, Y. Liang, T. Zhang, P.X. Ma, B. Guo, Antibacterial adhesive injectable hydrogels with rapid self-healing, extensibility and compressibility as wound dressing for joints skin wound healing, Biomaterials 183 (2018) 185–199.

[22] S. Pechenov, B. Shenoy, M.X. Yang, S.K. Basu, A.L. Margolin, Injectable controlled release formulations incorporating protein crystals, J. Control. Release 96 (1) (2004) 149–158.
[23] D. Schweizer, I. Vostiar, A. Heier, T. Serno, K. Schoenhammer, M. Jahn, S. Jones, A. Piequet, C. Beerli, H. Gram, A. Goepferich, Pharmacokinetics, biocompatibility and bioavailability of a controlled release monoclonal antibody formulation, J. Control. Release 172 (3) (2013) 975–982.
[24] D. Schweizer, K. Schonhammer, M. Jahn, A. Gopferich, Protein-polyanion interactions for the controlled release of monoclonal antibodies, Biomacromolecules 14 (1) (2013) 75–83.
[25] I. Bajaj, R. Singhal, Poly (glutamic acid) – an emerging biopolymer of commercial interest, Bioresour. Technol. 102 (10) (2011) 5551–5561.
[26] T. Yamagata, M. Morishita, N.J. Kavimandan, K. Nakamura, Y. Fukuoka, K. Takayama, N.A. Peppas, Characterization of insulin protection properties of complexation hydrogels in gastric and intestinal enzyme fluids, J. Control. Release 112 (3) (2006) 343–349.
[27] R. Langer, N.A. Peppas, Advances in biomaterials, drug delivery, and bionanotechnology, AIChE J. 49 (12) (2003) 2990–3006.
[28] M. Laitaoja, J. Valjakka, J. Janis, Zinc coordination spheres in protein structures, Inorg. Chem. 52 (19) (2013) 10983–10991.
[29] J. Wang, K.M. Chua, C.-H. Wang, Stabilization and encapsulation of human immunoglobulin G into biodegradable microspheres, J. Colloid Interface Sci. 271 (1) (2004) 92–101.
[30] B. Demeule, C. Palais, G. Machaidze, R. Gurny, T. Arvinte, New methods allowing the detection of protein aggregates: a case study on trastuzumab, MAbs 1 (2) (2009) 142–150.
[31] J. Yang, C. Ng, H. Lowman, R. Chestnut, C. Schofield, B. Sandlund, J. Ernst, G. Bennett, V. Quarmby, Quantitative determination of humanized monoclonal antibody rhuMAb2H7 in cynomolgus monkey serum using a Generic Immunoglobulin Pharmacokinetic (GRIP) assay, J. Immunol. Methods 335 (1–2) (2008) 8–20.
[32] Z.K. Kuo, M.W. Lin, I.H. Lu, H.J. Yao, H.C. Wu, C.C. Wang, S.H. Lin, S.Y. Wu, T.S. Tong, Y.C. Cheng, J.H. Yen, C.H. Ko, S.J. Chiou, I.H. Pan, H.W. Tseng, Antiangiogenic and antihepatocellular carcinoma activities of the Juniperus chinensis extract, BMC Complement. Altern. Med. 16 (2016) 277.
[33] I.R. Khalil, V.U. Irorere, I. Radecka, A.T.H. Burns, M. Kowalczuk, J.L. Mason, M.P. Khechara, Poly-gamma-glutamic acid: biodegradable polymer for potential protection of beneficial viruses, Materials (Basel) 9 (1) (2016).
[34] B.D. Mather, K. Viswanathan, K.M. Miller, T.E. Long, Michael addition reactions in macromolecular design for emerging technologies, Prog. Polym. Sci. 31 (5) (2006) 487–531.
[35] S.C. Rizzi, J.A. Hubbell, Recombinant protein-co-PEG networks as cell-adhesive and proteolytically degradable hydrogel matrixes. Part I: Development and physicochemical characteristics, Biomacromolecules 6 (3) (2005) 1226–1238.
[36] C.E. Espinosa-de la Garza, M.P. Miranda-Hernandez, L. Acosta-Flores, N.O. Perez, L.F. Flores-Ortiz, E. Medina-Rivero, Analysis of therapeutic proteins and peptides using multiangle light scattering coupled to ultra high performance liquid chromatography, J. Sep. Sci. 38 (9) (2015) 1537–1543.
[37] N.A. Peppas, Analysis of Fickian and non-Fickian drug release from polymers, Pharm. Aca Helvetiae 60 (4) (1985) 110–111.
[38] L.C. Costello, R.B. Franklin, Cytotoxic/tumor suppressor role of zinc for the treatment of cancer: an enigma and an opportunity, Expert Rev. Anticancer Ther. 12 (1) (2012) 121–128.
[39] H. Kocdor, H. Ates, S. Aydin, R. Cehreli, F. Soyarat, P. Kemanli, D. Harmanci, H. Cengiz, M.A. Kocdor, Zinc supplementation induces apoptosis and enhances antitumor efficacy of docetaxel in non-small-cell lung cancer, Drug Des. Dev. Ther. 9 (2015) 3899–3909.